This is a repository copy of *Competitive binding of Cd, Ni and Cu on goethite organo-mineral composites made with soil bacteria.*.

Article:

Competitive binding of Cd, Ni and Cu on goethite organo–mineral composites made with soil bacteria

Huihui Du, [1,2,]* Qiaoyun Huang, [2] Caroline L. Peacock, [3] Boqing Tie, [1] Ming Lei, [1] Xiaoli Liu, [1] Xiangdong Wei, [1]

[1] College of Resources and Environment, Hunan Agricultural University, Changsha 410128, P R China

[2] State Key Laboratory of Agricultural Microbiology, College of Resources and Environment, Huazhong Agricultural University, Wuhan 430070, PR China

[3] University of Leeds, School of Earth and Environment, Leeds, LS2 9JT, UK

*Corresponding Author: Huihui Du (Dr.)

Email: duhuihui@hunau.edu.cn;

Phone numbers: +86 0731-84618034

Postal address: 1st Nongda Road, Furong District, Changsha City, PR China.

ABSTRACT

Soil is a heterogeneous porous media that is comprised of a variety of organo-mineral aggregates. Sorption of heavy metals onto these composite solids is a key process that controls heavy metal mobility and fate in the natural environment. Pollution from a combination of heavy metals is common in soil, therefore, understanding the competitive binding behavior of metal ions to organo-mineral composites is important in order to predict metal mobility and fate. In this study, batch experiments were paired with spectroscopic studies to probe the sorption characteristics of ternary Cd-Ni-Cu sorbates to a binary organo-goethite composite made with *Bacillus cereus* cells. Scanning electron microscopy shows that goethite nano-sized crystals are closely associated with the bacterial surfaces. Sorption experiments show a larger adsorptivity and affinity for Cu than Cd/Ni on goethite and *B. cereus,* and the goethite–*B. cereus* composite. X-ray photoelectron spectroscopy reveals that carboxylate and phosphate functional moieties present on the bacterial cell walls are primarily responsible for metal sorption to the goethite–*B. cereus* composite. Synchrotron-based X-ray fluorescence shows that Cu and Ni are predominately associated with the bacterial fraction of the goethite–*B. cereus* composite, whereas Cd is mainly associated with the goethite fraction. The findings of this research have important implications for predicting the mobility and fate of heavy metals in soil multi-component systems.

Capsule abstract: Cd, Ni and Cu ions compete for similar binding sites on the

47 end-member goethite and *B. cereus*, but due to different binding affinities, Cu and Ni

48 are mainly bound to the bacterial fraction whereas Cd is predominately sorbed on the

49 goethite fraction of the binary bacteria–mineral composite.

50

53

54 **1. INTRODUCTION**

55   Heavy metal pollution in soils has received a lot of attention over recent decades,

56 due to the toxicity and persistence of heavy metals in the environment. A recent report

57 shows that Cd, Ni and Cu rank among the top three most serious heavy metal

58 pollutants on the Chinese mainland, with 7.0%, 4.8% and 2.1%, respectively, of

59 Chinese soils exceeding the Environmental Quality Standard for Soils in China (Zhao

60 et al., 2015). The mobility and fate of heavy metals in contaminated soils depends

61 largely on their sorption to various solid components, namely clay-sized minerals and

62 organic constituents such as humic substances, and bacterial and fungal biomass (Dai

63 et al., 2017; Du et al., 2016a). Moreover, multi-metal pollution is common, therefore,

64 the competitive or synergistic sorption of metal ions needs to be better understood in

65 order to properly predict heavy metal mobility and fate (Hughes et al., 2017; Yang et

66 al., 2016; Zhu et al., 2017).

67   With the ongoing development of spectroscopy techniques, the binding

68 characteristics of heavy metals on soil components have become increasingly clear. In

69   general, heavy metals sorb on minerals and organic components through non-specific

70   or specific sorption via the formation of either outer-sphere or inner-sphere complexes

71   (Bradl, 2004). Sorption of heavy metals to minerals and organic components is largely

72   dependent on pH, ionic strength, solid-to-metal ratio, temperature and the presence of

73   anionic ligands that are abundant in soil solutions (Du et al., 2018a; Peng et al., 2017).

74   In multi-metal contaminated environments, the sorption of individual heavy metals is

75   also affected by competition for sorption sites from other heavy metals. For example,

76   in clay sorption systems, Cu reduces Ni sorption on montmorillonite, but Ni exerts a

77   negligible effect on Cu sorption (Yang et al., 2015). The selective sorption sequence

78   of Cu>Ni can be attributed to differences in metal properties and the affinity of each

79   metal towards the montmorillonite binding sites. In organic sorption systems, Fowle

80   and Fein (1999) showed that sorption edges for Cu on *Bacillus subtilis* bacterial cells

81   occur at lower pH values compared to Cd, signifying the selective sorption sequence

82   of Cu>Cd for the organic bacterial cell surface sites. In mixed mineral and organic

83   sorption systems, the presence of organics can change the sorption behaviour of heavy

84   metals. For example, in a calcareous soil, the selectivity sequence of metal adsorption

85   is Cu>Cd>Ni (Jalali and Moradi, 2013), however, when soil is rich in organic matter,

86   the metal binding sites are more selective for Ni than Cd (Chorom et al., 2013).

87   Soil minerals and organics are commonly found to interact with one another to

88   produce organo-mineral composites (Kleber et al., 2015). For example, it is reported

89   that 50–75% of soil organic matter exists within clay-sized organo-mineral aggregates

90   (Christensen, 2001), and in particular ~21% of the organic carbon in sediments

91 appears to be associated with reactive iron phases (Lalonde et al., 2012).

92 Organo-mineral associations may arise through a number of processes, including the

93 formation of authigenic minerals promoted by organics (Gauger et al., 2016; Liu et al.,

94 2016), the coprecipitation of Fe/Al hydroxides in the presence of dissolved organic

95 compounds (Du et al., 2018b; Gentsch et al., 2015; Otero-Fariña et al., 2018), and the

96 adsorption of organics or formation of biofilms on mineral surfaces (Chen et al., 2014;

97 Playter et al., 2017). These processes lead to the formation of organo–mineral

98 composites, which exhibit different metal sorption behaviors compared to their

99 isolated end-member components. This in turn has lead to an increasing interest in the

100 binding behaviors of trace metals on various organo-mineral composites such as

101 organo–iron (hydr)oxides (Du et al., 2018a; Moon and Peacock, 2012, 2013;

102 Otero-Fariña et al., 2017, 2018), organo–silicate clay minerals (Du et al., 2017a;

103 Wang et al., 2016), organo–aluminum hydroxide (Du et al., 2018c), and organo–

104 manganite oxide composites (Pena et al., 2011). Results have shown that the organics

105 (e.g., humics, bacteria, etc.) play an important role in metal uptake at mid-low

106 environmental pH (Moon and Peacock, 2012), and also influence metal distribution

107 (Du et al., 2016a; 2017a; Moon and Peacock, 2012). However, to date, very little

108 information is available regarding multi-metal sorption behavior on mineral–organic

109 composites, despite the fact that soil solutions typically contain a mixture of metals. A

110 recent study by Zhu et al. (2012) shows that the competition between Cu and Cr for

111 sorption sites is stronger on a goethite–*B. thuringiensis* composite than on pure

112 goethite. In contrast however, a similar study found that the competition between Pb

113 and Cd on a pure clay mineral is stronger than on a clay mineral–*P. putida* composite

114 (Du et al., 2016b). These few available studies, from a macroscopic point of view,

115 suggest that mineral–organic interaction affects the competitive binding behaviors of

116 metals. However, microscopic information necessary to better understand this

117 competitive binding behavior, such as the metal coordination chemistry and the metal

118 distribution between the organic and mineral components in these complex systems, is

119 still poorly understood. Indeed, ternary-metal competition on organo-mineral

120 composites has never been studied.

121   This work investigates the competitive sorption characteristics of ternary

122 Cd-Ni-Cu sorbates on a model binary organo-mineral composite, i.e., a composite of

123 goethite and *Bacillus cereus* cells. Goethite is the most common iron oxide in the soil

124 environment and strongly interacts with various soil organic components including

125 microorganisms. *B. cereus* is a heavy metal resistant bacterium isolated from a

126 contaminated soil. Batch sorption combined with X-ray photoelectron spectroscopy

127 (XPS) and synchrotron-based X-ray fluorescence (μ-SRXRF) are employed to

128 determine macro and micro-level sorption information, towards a clearer

129 understanding of the metal-composite interactions. The results are important for better

130 prediction of the transport and fate of heavy metals in complex soil systems.

131

132 **2. MATERIALS AND METHODS**

133 *2.1 Sample preparation and characterization*

134   Goethite was synthesized by hydrolysis of a 0.1 M $Fe(NO_3)_3$ solution held at

135 60 °C for 24 h (Du et al., 2017b). *Bacillus cereus* is a Gram-positive bacterium,

136 isolated from a heavy metal contaminated soil. Its GenBank accession number is

137 MH345838 (NCBI, http://www.ncbi.nlm.nih.gov). The Luria-Bertani liquid medium

138 (10 g L^{-1} tryptone, 5 g L^{-1} yeast extract, 5 g L^{-1} NaCl) was used for bacterial

139 cultivation to the late-exponential phase. The cells were harvested by centrifugation

140 (4000 *g*) and washed several times with 0.1 M NaNO$_3$ (the electrolyte used in the

141 study). The goethite–*B. cereus* binary composite was prepared by adsorption of

142 bacterial cells to the mineral surface. Briefly, goethite and *B. cereus* were first

143 suspended in 0.1 M NaNO$_3$ under stirring. The bacterial suspension was then added

144 slowly to the mineral suspension, and allowed to react for 2 h until adsorption

145 equilibrium (Hong et al., 2012). The mass fraction of bacteria-to-mineral in the

146 composite was 50%:50% (dry mass), in order to maximize comparison of the metal

147 sorption beaviours between the composite and the isolated end-member goethite and

148 *B. cereus* cells.

149 Before metal sorption, the *B. cereus* cells were stained with fixable viability dye

150 and the fluorescence was measured using an Axio Imager A1M upright microscope

151 (Carl Zeiss Shanghai Co., Ltd.) to determine their bioactivity behavior, following the

152 method described by Wu et al. (2014). The results in Fig. S1 show that the *B. cereus*

153 cells were alive before the sorption of metal ions. The Brunauer-Emmett-Teller (BET)

154 specific surface area (SSA) of goethite was measured by nitrogen adsorption using an

155 automated gas sorption analyzer (Autosorb-IQ, Quantachrome, US). The morphology

156 of the goethite, *B. cereus* cells and goethite–*B. cereus* composite was characterized by

157 scanning electron microscopy (SEM) coupled with energy-dispersive spectroscopy

158 (FE-SEM/EDS, Quanta F250, Germany). For SEM-EDS, the samples were fixed in

159 2.5% glutaraldehyde, subjected to an ethanol dehydration series, and dried in a freezer

160 dryer at –53 °C.

161

162 *2.2 Sorption experiments*

163 Sorption isotherm experiments were carried out in a batch process at 25 °C. The stock

164 solutions of Cd(II), Ni(II) and Cu(II) were prepared at 10 mM from analytically pure

165 $Cd(NO_3)_3$, $Ni(NO_3)_3$ and $Cu(NO_3)_3$, respectively. Sorption samples were prepared by

166 mixing known amounts of goethite, *B. cereus* or goethite–*B. cereus* composite

167 suspensions with Cd(II), Ni(II) or Cu(II) solutions (single-metal sorption systems) and

168 mixed Cd(II), Ni(II) and Cu(II) solutions (ternary-metal sorption systems; the initial

169 molar ratio was 1:1:1). The final sorption suspension contained 1 g L^{-1} sorbent and 0–

170 0.5 mM metal ions. Suspension pH was set to 5.5 by minor additions of either HNO_3

171 or NaOH. This mildly acidic pH was chosen to best represent the pH of most common

172 soil types (i.e., red soil) in southern China (Xu et al., 2003), where soil multi-heavy

173 metal contamination is a serious environmental problem (Li et al., 2010). At this pH

174 Cd, Ni and Cu occur predominantly as free aqueous divalent ions with no

175 precipitation of metal (hydr)oxides (Du et al., 2017a; Moon and Peacock, 2012; Tan et

176 al., 2011). The mixtures were shaken continuously for 24 h during which time the pH

177 was recorded and subsequently adjusted to the set pH every 4 h. All sorption

178 suspensions were separated by centrifugation (8000 *g*) into to clear supernates for

179   analyses of total Cd, Ni and Cu by atomic absorption spectroscopy (AAS, Varin

180   AAS240FS) and a thick paste for SEM-EDS, XPS and μ-SRXRF analysis.

181

182   *2.3 X-ray photoelectron spectroscopy*

183   The goethite–*B. cereus* composite before and after sorption of Cd, Ni and Cu was

184   analysed via X-ray photoelectron spectroscopy (XPS) using a multifunctional imaging

185   electron spectrometer (Thermo ESCALAB 250XI) with monochromatic Al Ka

186   radiation (1486.6 eV). For each sample, the data were collected over an energy range

187   0–1350 eV on an area 500 μm × 500 μm. The step size for the wide survey scan and

188   high-resolution scan was 1 eV and 0.05 eV, respectively. Binding energies were

189   calibrated using the C 1s peak (284.8 eV). A software package, XPSPEAK41, was

190   used to fit the XPS spectral peaks. The full width at half-maximum (FWHM) was

191   maintained constant in any particular spectrum.

192

193   *2.4 Synchrotron-based X-ray imaging*

194   The elemental distribution of Cd, Ni and Cu within the goethite–*B. cereus*

195   composite was characterized by synchrotron-based X-ray fluorescence. The thick

196   pastes that were separated from the sorption suspensions were collected and stored at

197   4 °C to reduce drying during shipment to the Shanghai Synchrotron Radiation Facility

198   (SSRF). All the μ-SRXRF measurements were conducted within 24 h of the sorption

199   experiments. The BL15U1 beamline of the SSRF is a hard X-ray micro-focusing

200   beamline for X-ray fluorescence (XRF), which allows a non-destructive investigation

of the spatial distribution of target trace elements correlated to the morphology of the

sample at a resolution of a few micrometers (Du et al., 2016b). The storage ring

energy was 3.5 GeV and the beam current varied between 200–300 mA during the

measurements. Fluorescence signals were collected using a multi-element Si(111)

detector with a beam spot size of 2 μm × 2 μm. Herein, P (as a basic element for

bacterial growth) and Fe signals were chosen to represent the bacterial and mineral

component in the composite, respectively (Du et al., 2016b; Kemner et al., 2004).

Data processing was accomplished using the Igorpro 6.10 (WaveMatrics, Inc.)

software (Du et al., 2016b). The point source data for Cu, Ni, Cd, P and Fe were

extracted to allow correlation analysis using the SPSS 19.0 program.

3. RESULTS

3.1 Characterization of goethite, B. cereus and their organo-mineral composite

The synthesized goethite in this study is the same batch as that used in our

previous work (Du et al., 2017b), and its XRD pattern matches that of standard

goethite (JCPDS card NO. 29-0713). The SSA of the goethite was determined by N_2

adsorption as 18.3 ± 0.2 m^2 g^{-1}. The SEM images of goethite, *B. cereus* cells and

goethite–*B. cereus* composite are shown in Fig. 1. Goethite possesses well-developed

acicular crystals that are aggregated together (Fig. 1a). The length of the crystals is

typically several hundreds of nanometers. *Bacillus cereus* cells are rod-shaped, and

about 3 μm long and 1 μm wide (Fig. 1b). SEM of the goethite–*B. cereus* composite

shows that the cells are intact, and the goethite crystals are closely associated with the

223 cells, giving rise to a mineral film on the outer surface of the cells, as opposed to a

224 biofilm on the mineral surface (Fig. c and d). This kind of association is commonly

225 found in metal oxide–bacteria composite systems (Du et al., 2018b; Templeton et al.,

226 2003), mainly due to the smaller particle size of the mineral crystals compared to the

227 bacterial cells and the opposing surface charges of the end-member components that

228 results in their electrostatic attraction (Jiang et al., 2007).

229

230 *3.2 Sorption isotherms*

231 The sorption isotherms for the different sorbents are shown in Fig. 2. The

232 experimental sorption data are well fit by a Langmuir equation as follows:

233
$$q_e = \frac{q_m K C_e}{1 + K C_e} \quad (1)$$

234 where q_e represents the adsorption amount at equilibrium concentration of C_e after

235 adsorption, q_m represents the maximal adsorption capacity and K is the binding

236 affinity. The Langmuir model has been successfully applied to describe the

237 competitive sorption isotherms of heavy metals on soil minerals and organo-mineral

238 composites (Du et al., 2016b; Komarek et al., 2015; Zhu et al., 2012). The goodness

239 of the fits in Table 1 ($R>0.92$) suggests that this model is suitable for quantifying

240 sorption in the studied systems.

241 In single-metal systems, the maximum sorption of Cd, Ni and Cu on goethite is

242 53.82, 49.11 and 77.79 mmol kg^{-1}, respectively, compared to 165.63, 194.32 and

243 224.74 mmol kg^{-1} on *B. cereus* (Table 1). It is evident that *B. cereus* cells exhibit a

244 higher metal sorption capacity than pure goethite, possibly owing to the abundant

245   functional groups on bacterial cell walls (Fein et al., 1997). The maximum sorption

246   (q_m) and binding affinity (K) follows the order Cu>Cd $\approx$ Ni on goethite, and

247   Cu>Ni>Cd on *B. cereus*, and thus our results show that Cu is preferentially sorbed

248   over Ni and Cd by both the mineral and organic sorbents, and Ni is preferentially

249   sorbed over Cd on the bacterial cell surface. The goethite–*B. cereus* composite shows

250   intermediate metal sorption behavior between end-member goethite and *B. cereus*.

251   The maximum sorption of Cd, Ni and Cu on the composite is 128.15, 134.24 and

252   179.04 mmol kg^{-1}, respectively.

253   In ternary-metal systems, metal sorption decreases compared to sorption in the

254   absence of competing metal ions (Fig. 2). By comparison, the sorption (q_m) of Cd is

255   reduced by ~61% on goethite, 51.3% on *B. cereus* and 55.1% on the goethite–*B.*

256   *cereus* composite; the sorption of Ni is reduced by ~59.0% on goethite, 48.8% on *B.*

257   *cereus* and 48.8% on the goethite–*B. cereus* composite; while the sorption of Cu is

258   reduced by ~26.0% on goethite, 14.5% on *B. cereus* and 22.5% on the goethite–*B.*

259   *cereus* composite. There reduction in metal sorption on goethite as a result of

260   competitive sorption is greater than that observed for *B. cereus* and the goethite–*B.*

261   *cereus* composite, possibly due to the smaller number of surface sorption sites on

262   goethite compared to *B. cereus* cells. It is also worth noting that the values of the

263   binding affinities (K) in the ternary-metal systems are larger than those in the

264   single-metal systems, implying that heavy metals sorb on higher affinity sorption sites

265   in the presence of competing metals.

266

3.3 XPS analysis

268   X-ray photoelectron spectra over the energy range 0–1350 eV are shown in Fig.

269 3a and confirm that the goethite–*B. cereus* composite comprises an elemental

270 composition arising from both the mineral (e.g., Fe, O) and bacterial fraction (e.g., C,

271 O, N, P) with very small peaks of Cu 2p (~932 eV), Ni 2p (~852 eV) and Cd 3d (~404

272 eV) present after metal sorption (Fig. 3b). XPS peaks corresponding to C and O were

273 analyzed at high resolution to assess the contributions from different components that

274 comprise these peaks (Fig. 4). Herein, the carbon peak was fit into three components

275 as follows: carbon bound to carbon and hydrogen, C–(C, H), at ~284.9 eV; carbon

276 bound to oxygen or nitrogen from alcohols, amines and/or amides, C–(O, N), at

277 ~286.4 eV; and carbon doubly bound to one oxygen or singly bound to two oxygens

278 (C=O, O–C–O, at ~287.9 eV) attributable to the carbonyls, carboxylates and/or

279 aldehydes (Ojeda et al., 2008; Omoike and Chorover, 2004) (Fig. 4a and b). These

280 components are abundant in the phospholipid bilayer, peptidoglycan, teichoic acid,

281 lipopolysaccharid and protein of the *B. cereus* cell wall. It is interesting that the

282 component at ~287.9 eV decreases by ~20.7% when the goethite–*B. cereus* composite

283 sorbs Cd, Ni and Cu (Fig. 4a and b). This suggests that carboxylic and amino groups

284 play an important role in the uptake of metal ions on the goethite–*B. cereus* composite.

285 The oxygen peak was decomposed into three components: oxygen doubly bound to

286 carbon or phosphorus from carboxylates and phosphoryls, C=O/C=P, at ~530.4 eV;

287 oxygen bound to hydrogen from FeOOH, O–H, at ~531.3 eV; and oxygen singly

288 bound to carbon from alcohols or carbon singly bound to two carbons from acetals

289   and hemiacetals, O–C and C–O–C, at ~532.7 eV (Abdel-Samad and Watson, 1997;

290   Ahimou et al., 2007) (Fig. 4c and d). We find that the component at ~530.4 eV

291   decreases from 10.1% to 7.9% when the goethite–*B. cereus* composite sorbs Cd, Ni

292   and Cu, while the component at ~531.1 eV is almost unchanged. This suggests that

293   Cd, Ni and Cu are predominately bound to the carboxylic and phosphoryl groups of

294   the bacterial cells. Taken together, the C 1s and O 1s peak fitting results suggest that

295   metal ions are predominately bound to the bacterial fraction of the goethite–*B. cereus*

296   composite.

297

298   *3.4 Elemental distribution*

299   To further investigate the spatial distribution of the sorbed metals, the goethite–*B.*

300   *cereus* composite after sorbing Cd, Ni and Cu was analysed with SEM-EDS and

301   µ-SRXRF. These two techniques combined can provide information on the content

302   and location of Cd, Ni and Cu, and so can determine the distribution of the sorbed

303   metals between the bacterial and mineral fractions in the composite. The strong C, O

304   and Fe peaks in Fig. 1e suggest that the studied area comprises both bacterial cells and

305   goethite while the presence of small Cd, Ni and Cu peaks signifies the uptake of these

306   three metals by the goethite–*B. cereus* composite. The mass percentage of Cd, Ni and

307   Cu in the studied area is 0.88%, 1.16% and 1.97%, respectively, corresponding to an

308   atomic percentage of 0.1%, 0.26% and 0.41%, respectively. The order of abundance

309   of the sorbed metals on the goethite–*B. cereus* composite is therefore Cu>Ni>Cd. This

310   agrees with the order of abundance measured for the single metal sorption systems

311 (Fig. S2), and is in accord with the batch sorption results (Fig. 2).

312   While SEM-EDS can provide information on the absolute content of elements in

313 a sample, it is incapable of providing information on how these elements are

314 distributed between the bacterial and mineral fractions in the goethite–*B. cereus*

315 composite. Recently, synchrotron-based XRF has emerged as a powerful technique to

316 probe the distribution of elements in complex samples such as natural soils and

317 sediments (Cumberland et al., 2018; Yu and Lu, 2016), plants (El Hayek et al., 2017;

318 Lu et al., 2017) and organo-mineral composites (Du et al., 2016b). The synchrotron

319 XRF data for Fe, P, Cu, Ni and Cd in the goethite–*B. cereus* composite are shown in

320 Fig. 5. In accord with the SEM-EDS and batch sorption results, the fluorescence

321 intensity (counts) for Cu are larger than that for Ni and Cd in the goethite–*B. cereus*

322 composite. As for the XPS analysis, we use Fe and P to represent the goethite and

323 bacterial fractions of the composite, respectively (Kemner et al., 2004). Given this, we

324 see that Cu-enriched areas are concentrated with P (correlation coefficient 0.574),

325 while a noticeable fraction of Cu is negatively correlated with Fe (correlation

326 coefficient 0.387). This implies that Cu is mainly associated with the bacterial fraction

327 in the goethite–*B. cereus* composite. Similarly, Ni is enriched in the lower-middle

328 parts of the samples where P is enriched and there is a higher correlation with P

329 (r=0.268) than Fe (r=0.137), suggesting that Ni is also mainly sorbed on the bacterial

330 fraction of the composite. In contrast however, Cd distribution is similar to that of Fe

331 as opposed to P with a much higher correlation coefficient with Fe (r=0.424) than P

332 (r=0.144), suggesting that Cd is mainly sorbed on the goethite fraction of the

333 composite.

334

335 **4. DISCUSSION**

336   Our results show that the sorption of Cd, Ni and Cu on goethite, *B. cereus* and a

337 goethite–*B. cereus* binary composite is suppressed in the presence of competing

338 metals. In particular, Cu shows a much greater capacity and affinity towards both the

339 mineral and organic surface than Cd and Ni according to the macro- and micro-level

340 information. The selective sorption of Cu on the sorbent surfaces can be ascribed to

341 the differences in the properties of Cd, Ni and Cu, where Cu hydrolyzes more readily

342 and has a smaller hydrated radius, compared to Cd and Ni, and hence its interaction

343 with a deprotonated surface is favoured (Srivastava et al., 2005). This selective

344 sorption order of Cu>Cd/Ni has also been observed in other soil sorption systems

345 (Covelo et al., 2004; Srivastava et al., 2005; Yang et al., 2015). It is noteworthy that

346 Cd and Ni, however, show contrasting sorption behaviours in the goethite–*B. cereus*

347 composite sorption system, i.e., Cd is preferentially sorbed to the mineral fraction

348 whereas Ni is preferentially sorbed to the bacterial fraction. This phenomena is

349 probably again due to the differences in the properties of Cd and Ni and thus their

350 binding affinities on the organic functional group sorption sites. According to the

351 Pearson classification of metals (Pearson, 1969), Cd^{2+} is a "soft" metal and thus forms

352 more stable complexes with soft donors such as sulfhydryl and amino groups, whereas

353 Ni^{2+} is a more "hard" or non-polarizable metal and thus forms more stable complexes

354 with hard donors such as carboxylate, carbonate, phosphate and hydroxyl groups

355 (Karakagh et al., 2012; Williams et al., 1998). Because our XPS indicates that

356 carboxyl- and phosphoryl-metal complexation is the most probable metal-binding

357 mechanism on the bacterial cells and the bacterial fraction of the goethite–*B. cereus*

358 composite, it is expected that Ni will show a higher affinity towards the bacterial

359 fraction of the composite compared to Cd, resulting in more bacteria-associated Ni

360 and relatively less bacteria-associated Cd. This assumption is further confirmed by the

361 XPS results for the composite with sorbed Ni or Cd (Fig. S3), which show that the

362 reduction in the C=O/P=O component is larger for Ni than Cd, whereas the reduction

363 in the Fe–O–H component is smaller for Ni than Cd. Higher biosorption of Ni

364 compared to Cd has also been found for other bacterial strains such as *Actinomyces* sp.

365 and *Streptomyces* sp. (Karakagh et al., 2012).

366 This study suggests that Cd, Ni and Cu ions compete for similar binding sites on

367 end-member goethite and bacterial cells, and thus on goethite-bacteria composites, but

368 the available binding sites may have a different affinity for specific metal ions. This

369 could have an important impact on the eventual fate of Cd, Ni and Cu in natural and

370 contaminated soil systems. In particular, in acid polluted soils such as red soil, Cd is

371 often present along with much higher concentrations of Ni and Cu, and in these

372 systems Cd will likely bind to the goethite fraction rather than the organic fraction of

373 the soil organo-mineral composites. This has important implications for the

374 physico-chemical and biological remediation of Cd-contaminated soils.

375 This study also reports that competitive sorption between different heavy metals

376 in the goethite–bacteria composite sorption system is less intense compared to that

377 observed in the end member mineral sorption system. This finding is similar to recent

378 work showing that the competitive sorption of Pb and Cd on a clay mineral–bacteria

379 composite is less intense than on the pure clay mineral (Du et al., 2016b). Our work

380 on the competitive sorption of heavy metals to mineral-bacterial composites adds to

381 recent work on the sorption of individual metals to similar mineral-bacteria

382 composites where minerals with sorbed bacteria show different metal binding

383 behaviors, compared to the pure mineral counterparts (Moon and Peacock, 2012,

384 2013). In particular, our competitive sorption work has important implications for

385 elucidating the mobility and fate of heavy metals in complex soil environments. For

386 example, in areas of the soil system that are organic rich, such as the soil-plant

387 interface, abundant bacterial and fungal biomass is spatially associated with minerals,

388 and current predictions of metal behaviour based on pure mineral systems might

389 over-estimate the intensity of competitive sorption on mineral-bacterial composites,

390 and thus under-estimate the total metal sorption at the composite interface.

391 Furthermore, with different binding affinities towards the different composite

392 fractions, the distribution of different metals between the mineral and bacterial

393 fractions in complex soil aggregates will be quite different. As such the mineral-bound

394 and organic-bound metals may show different behaviors during many soil processes,

395 for example, the mineral-bound metals may be sensitive to soil acidification while the

396 mobility of organic-bound metals may increase during organic decomposition into

397 low molecular weight organic ligands. In this scenario, as above, it will be important

398 to consider multi-metal sorption competition on mineral–bacteria composites, in order

399 to predict metal mobility and fate in multi-metal contaminated soil environments. This

400 study focused on a relatively simple multi-metal competitive sorption system, but soil

401 is a complex ecosystem whose chemical, biological and geological state is highly

402 variable, therefore several issues such as the effects of pH and ionic strength, and

403 bacteria-to-mineral ratio on multi-metal sorption should be addressed in a further

404 study.

405

406 5. CONCLUSIONS

407 We show that cells of *Bacillus cereus* can closely associate with goethite to form a

408 binary mineral–bacteria composite, in which the mineral particles form a mineral film

409 on the surface of the bacterial cell walls. We see that *B. cereus* cells are more effective

410 for the removal of Cd, Ni and Cu from solution than goethite, while the goethite–*B.*

411 *cereus* composite shows intermediate metal sorption behaviours between the

412 end-member goethite and *B. cereus* cells. The isothermal sorption data conforms to

413 the Langmuir model with the adsorptivities on goethite and *B. cereus* following the

414 orders Cu>Cd≈Ni and Cu>Ni>Cd, respectively. Carboxylate- and phosphate-binding

415 is the primary sorption mechanism for the metals on the goethite–*B. cereus* composite.

416 Overall Cu and Ni are mostly sequestered by the bacterial fraction, while in contrast,

417 more Cd is sorbed on the goethite fraction of the mineral–bacteria composite. Our

418 observations have important implications for predicting the sorption, mobility and fate

419 of multi-metals at complex soil interfaces.

420

References

(1) Abdel-Samad, H., Watson, P.R., 1997. An XPS study of the adsorption of chromate on goethite (α -FeOOH). Appl. Surf. Sci. 108, 371-377.

(2) Ahimou, F., Boonaert, C.J., Adriaensen, Y., Jacques, P., Thonart, P., Paquot, M., Rouxhet, P.G., 2007. XPS analysis of chemical functions at the surface of *Bacillus subtilis*. J. Colloid Interf. Sci. 309, 49-55.

(3) Bradl, H.B., 2004. Adsorption of heavy metal ions on soils and soils constituents, J. Colloid Interf. Sci. 277, 1–18.

(4) Chen, C., Dynes, J.J., Wang, J., Sparks, D.L., 2014. Properties of Fe-organic matter associations via coprecipitation versus adsorption. Environ. Sci. Technol. 48, 13751-13759.

(5) Chorom, M., Karkaragh, R.M., Kaviani, B., Kalkhajeh, Y.K., 2013. Monometal and competitive adsorption of Cd, Ni, and Zn in soil treated with different contents of cow manure. Appl. Environ. Soil Sci. 2013, 510278.

(6) Christensen, B.T., 2001. Physical fractionation of soil and structural and functional complexity in organic matter turnover. Eur. J. Soil Sci. 52, 345-353.

(7) Covelo, E.F., Andrade, M.L., Vega, F.A., 2004. Heavy metal adsorption by humic umbrisols: selectivity sequences and competitive sorption kinetics. J. Colloid Interf. Sci. 280, 1-8.

447   (8) Cumberland, S.A., Etschmann, B., Brugger, J., Douglas, G., Evans, K., Fisher, L., Kappen, P.,

448   Moreau, J.W., 2018. Characterization of uranium redox state in organic-rich Eocene

449   sediments. Chemosphere 194, 602-613.

450   (9) Dai, C., Lin, M.X., Hu, Y.D., 2017. Heterogeneous Ni- and Cd-bearing ferrihydrite

451   precipitation and recrystallization on quartz under acidic pH condition. ACS Earth Space

452   Chem. 1, 621-628.

453   (10) Du, H., Chen, W., Cai, P., Rong, X., Dai, K., Peacock, C.L., Huang, Q., 2016a. Cd(II)

454   sorption on montmorillonite-humic acid-bacteria composites. Sci. Rep. 6, 19499.

455   (11) Du, H., Chen, W., Cai, P., Rong, X., Feng, X., Huang, Q., 2016b. Competitive adsorption of

456   Pb and Cd on bacteria–montmorillonite composite. Environ. Pollut. 218, 168-175.

457   (12) Du, H., Qu, C., Liu, J., Chen, W., Cai, P., Shi, Z., Yu, X.Y., Huang, Q., 2017a. Molecular

458   investigation on the binding of Cd(II) by the binary mixtures of montmorillonite with two

459   bacterial species. Environ. Pollut. 229, 871-878.

460   (13) Du, H., Lin, Y., Chen, W., Cai, P., Rong, X., Shi, Z., Huang, Q., 2017b. Copper adsorption on

461   composites of goethite, cells of *Pseudomonas putida* and humic acid. Eur. J. Soil Sci. 68,

462   514-523.

463   (14) Du, H., Peacock, C.L., Chen, W.. Huang, Q. 2018a. Binding of Cd by ferrihydrite

464   organo-mineral composites: Implications for Cd mobility and fate in natural and

465   contaminated environments. Chemosphere, 207, 404-412.

466   (15) Du, H., Huang, Q., Lei, M., Tie, B., 2018b. Sorption of Pb(II) by nanosized ferrihydrite

467   organo-mineral composites formed by adsorption versus coprecipitation. ACS Earth Space

468   Chem. 2, 556-564.

469   (16) Du, H., Huang, Q., Yang, R., Tie, B., Lei, M., 2018c. Cd sequestration by bacteria-aluminum

470   hydroxide composites. Chemosphere 198, 75-82.

471   (17) El Hayek, E., El Samrani, A., Lartiges, B., Kazpard, V., Aigouy, T., 2017. Lead

472   bioaccumulation in Opuntia ficus-indica following foliar or root exposure to lead-bearing

473   apatite. Environ. Pollut. 220, 779-787.

474   (18) Fein, J.B., Daughney, C.J., Yee, N., Davis, T.A., 1997. A chemical equilibrium model for

475   metal adsorption onto bacterial surfaces. Geochim. Cosmochim. Acta 61, 3319-3328.

476   (19) Fowle, D.A., Fein, J.B., 1999. Competitive adsorption of metal cations onto two gram

477   positive bacteria: testing the chemical equilibrium model. Geochim. Cosmochim. Acta 63,

478   3059-3067.

479   (20) Gauger, T., Byrne, J.M., Konhauser, K.O., Obst, M., Crowe, S., Kappler, A., 2016. Influence

480   of organics and silica on Fe(II) oxidation rates and cell–mineral aggregate formation by the

481   green-sulfur Fe(II)-oxidizing bacterium *Chlorobium ferrooxidans* KoFox – Implications for

482   Fe(II) oxidation in ancient oceans. Earth Planet. Sci. Let. 443, 81-89.

483   (21) Gentsch, N., Mikutta, R., Shibistova, O., Wild, B., Schnecker, J., Richter, A., Urich, T., Gittel,

484   A., Šantrůčková, H., Bárta, J., 2015. Properties and bioavailability of particulate and mineral-

485   associated organic matter in Arctic permafrost soils, Lower Kolyma Region, Russia. Eur. Soil

486   Sci. 66, 722-734.

487   (22) Hong, Z., Rong, X., Cai, P., Dai, K., Liang, W., Chen, W., Huang, Q., 2012. Initial adhesion

488   of *Bacillus subtilis* on soil minerals as related to their surface properties. Eur. J. Soil Sci. 63,

489   457-466.

490   (23) Hughes, D.L., Afsar, A., Harwood, L.M., Jiang, T., Laventine, D.M., Shaw, L.J., Hodson,

491   M.E., 2017. Adsorption of Pb and Zn from binary metal solutions and in the presence of

492   dissolved organic carbon by DTPA-functionalised, silica-coated magnetic nanoparticles.

493   Chemosphere 183, 519-527.

494   (24) Jalali, M., Moradi, F., 2013. Competitive sorption of Cd, Cu, Mn, Ni, Pb and Zn in polluted

495   and unpolluted calcareous soils. Environ. Monit. Assess. 185, 8831-8846.

496   (25) Jiang, D., Huang, Q., Cai, P., Rong, X., Chen, W., 2007. Adsorption of *Pseudomonas putida*

497   on clay minerals and iron oxide. Colloid Surface B. 54, 217-221.

498   (26) Karakagh, R.M., Chorom, M., Motamedi, H., Kalkhajeh, Y.K., Oustan, S., 2012. Biosorption

499   of Cd and Ni by inactivated bacteria isolated from agricultural soil treated with sewage

500   sludge. Ecohydrol. Hydrobiol. 12, 191-198.

501   (27) Kemner, K.M., Kelly, S.D., Lai, B., Maser, J., O'Loughlin E, J., Sholto-Douglas, D., Cai, Z.,

502   Schneegurt, M.A., Kulpa, C.F., Jr., Nealson, K.H., 2004. Elemental and redox analysis of

503   single bacterial cells by x-ray microbeam analysis. Science 306, 686-687.

504   (28) Kleber, M., Eusterhues, K., Keiluweit, M. Mikutta, M., Mikutta, M., Nico, P.s., 2015. Chapter

505   one–mineral–organic associations: formation, properties, and relevance in soil environments.

506   Adv. Agron. 130, 1-140.

507   (29) Komarek, M., Koretsky, C.M., Stephen, K.J., Alessi, D.S., Chrastny, V., 2015. Competitive

508   adsorption of Cd(II), Cr(VI), and Pb(II) onto nanomaghemite: A spectroscopic and modeling

509   approach. Environ. Sci. Technol. 49, 12851-12859.

510   (30) Lalonde, K., Mucci, A., Ouellet, A., Gelinas, Y., 2012. Preservation of organic matter in

511   sediments promoted by iron. Nature 483, 198-200.

512   (31) Li, Y., Ge, Y., Zhang, C., Zhou, Q., 2010. Mechanisms for high Cd activity in a red soil from

513   southern China undergoing gradual reduction. Soil Res. 48, 371-384.

514   (32) Liu, D., Zhang, Q.F., Wu, L.L., Zeng, Q., Dong, H.L., Bishop, M.E., Wang, H.M., 2016.

515   Humic acid-enhanced illite and talc formation associated with microbial reduction of Fe(III)

516   in nontronite. Chem. Geol. 447, 199-207.

517   (33) Lu, L., Xie, R., Liu, T., Wang, H., Hou, D., Du, Y., He, Z., Yang, X., Sun, H., Tian, S., 2017.

518   Spatial imaging and speciation of Cu in rice (Oryza sativa L.) roots using synchrotron-based

519   X-ray microfluorescence and X-ray absorption spectroscopy. Chemosphere 175, 356-364.

520   (34) Moon, E.M., Peacock, C.L., 2012. Adsorption of Cu(II) to ferrihydrite and ferrihydrite–

521   bacteria composites: Importance of the carboxyl group for Cu mobility in natural

522   environments. Geochim. Cosmochim. Acta 92, 203-219.

523   (35) Moon, E.M., Peacock, C.L., 2013. Modelling Cu(II) adsorption to ferrihydrite and

524   ferrihydrite–bacteria composites: Deviation from additive sorption in the composite sorption

525   system. Geochim. Cosmochim. Acta 104, 148-164.

526   (36) Ojeda, J.J., Romero-Gonzalez, M.E., Bachmann, R.T., Edyvean, R.G., Banwart, S.A., 2008.

527   Characterization of the cell surface and cell wall chemistry of drinking water bacteria by

528   combining XPS, FTIR spectroscopy, modeling, and potentiometric titrations. Langmuir 24,

529   4032-4040.

530   (37) Omoike, A., Chorover, J., 2004. Spectroscopic study of extracellular polymeric substances

531   from *Bacillus subtilis*: aqueous chemistry and adsorption effects. Biomacromolecules 5,

532   1219-1230.

533   (38) Otero-Fariña, A., Fiol, S., Arce, F., Antelo, J., 2017. Effects of natural organic matter on the

534   binding of arsenate and copper onto goethite. Chem. Geol. 459, 119-128.

535   (39) Otero-Fariña, A., Peacock, C.L., Fiol, S., Antelo, J., Carvin, B. 2018. A universal adsorption

536   behaviour for Cu on iron (hydr)oxide organo-mineral composites. Chem. Geol. 479, 22-35.

537   (40) Pearson, R.G., 1969. Hard and Soft Acids and Bases. Surv. Prog. Chem. 5, 1-52.

538   (41) Pena, J., Bargar, J.R., Sposito, G., 2011. Role of bacterial biomass in the sorption of Ni by

539   biomass-birnessite assemblages. Environ. Sci. Technol. 45, 7338-7344.

540   (42) Peng, H., Gao, P., Chu, G., Pan, B., Peng, J., Xing, B., 2017. Enhanced adsorption of Cu(II)

541   and Cd(II) by phosphoric acid-modified biochars. Environ. Pollut. 229, 846-853.

542   (43) Playter, T., Konhauser, K., Owttrim, G., Hodgson, C., Warchola, T., Mloszewska, A.M.,

543   Sutherland, B., Bekker, A., Zonneveld, J.P., Pemberton, S.G., Gingras, M., 2017.

544   Microbe-clay interactions as a mechanism for the preservation of organic matter and trace

545   metal biosignatures in black shales. Chem. Geol. 459, 75-90.

546   (44) Srivastava, P., Singh, B., Angove, M., 2005. Competitive adsorption behavior of heavy

547   metals on kaolinite. J. Colloid Interf. Sci. 290, 28-38.

548   (45) Tan, X., Hu, J., Montavon, G., Wang, X., 2011. Sorption speciation of nickel(II) onto

549   Ca-montmorillonite: batch, EXAFS techniques and modeling. Dalton Trans. 40,

550   10953-10960.

551   (46) Templeton, A.S., Spormann, A.M., Brown, G.E., 2003. Speciation of Pb (II) sorbed by

552   *Burkholderia cepacia*/goethite composites. Environ. Sci. Technol. 37, 2166-2172.

553   (47) Wang, N., Du, H., Huang, Q., Cai, P., Rong, X., Feng, X., Chen, W., 2016. Surface

554   complexation modeling of Cd(II) sorption to montmorillonite, bacteria, and their composite.

555   Biogeosciences 13, 5557-5566.

556   (48) Williams, C.J., Aderhold, D., Edyvean, R.G.J., 1998. Comparison between biosorbent for the

557   removal of metal ions from aqueous solutions. Water Res. 32, 216-224.

558   (49) Wu, H.Y, Chen, W.L., Rong, X.M., Cai, P., Dai, K., Huang, Q.Y., 2014. Adhesion of

559   *Pseudomonas putida* onto kaolinite at different growth phases. Chem. Geol. 390, 1-8.

560   (50) Xu, R., Zhao, A., Li, Q., Kong, X., Ji, G., 2003. Acidity regime of the red soils in a

561   subtropical region of southern China under field conditions. Geoderma 115, 75-84.

562   (51) Yang, S., Ren, X., Zhao, G., Shi, W., Montavon, G., Grambow, B., Wang, X., 2015.

563   Competitive sorption and selective sequence of Cu(II) and Ni(II) on montmorillonite: Batch,

564   modeling, EPR and XAS studies. Geochim. Cosmochim. Acta 166, 129-145.

565   (52) Yang, Y., Zhang, W., Qiu, H., Tsang, D.C.W., Morel, J.L., Qiu, R., 2016. Effect of coexisting

566   Al(III) ions on Pb(II) sorption on biochars: Role of pH buffer and competition. Chemosphere

161, 438-445.

(53) Yu, X., Lu, S., 2016. Multiscale correlations of iron phases and heavy metals in technogenic magnetic particles from contaminated soils. Environ. Pollut. 219, 19-27.

(54) Zhao, F.J., Ma, Y., Zhu, Y.G., Tang, Z., Mcgrath, S.P., 2015. Soil contamination in China: current status and mitigation strategies. Environ. Sci. Technol. 49, 750-759.

(55) Zhu, J., Huang, Q., Pigna, M., Violante, A., 2012. Competitive sorption of Cu and Cr on goethite and goethite–bacteria complex. Chem. Eng. J. 179, 26-32.

(56) Zhu, W., Du, W., Shen, X., Zhang, H., Ding, Y., 2017. Comparative adsorption of Pb^{2+} and Cd^{2+} by cow manure and its vermicompost. Environ. Pollut. 227, 89-97.

597

598   **Table 1**. Langmuir parameters for the adsorption of Cd, Ni and Cu in single and ternary

599   (competitive) systems on goethite, *B. cereus*, and *B. cereus*–goethite binary composite.

	metal	System	Langmuir model		
			$q_m{}^a$ (mmol kg^{-1})	K^b (L mol^{-1})	R^2
goethite	Cd	Cd alone	53.82	7.1	0.99
		Cd+Ni+Cu	21.01	7.6	0.99
	Ni	Ni alone	49.11	6.5	0.99
		Cd+Ni+Cu	20.12	15.3	0.98
	Cu	Cu alone	77.79	18.9	0.98
		Cd+Ni+Cu	57.52	28.0	0.98
B. cereus	Cd	Cd alone	165.63	28.0	0.99
		Cd+Ni+Cu	80.63	51.8	0.94
	Ni	Ni alone	194.32	46.6	0.92
		Cd+Ni+Cu	99.54	53.6	0.99
	Cu	Cu alone	224.74	72.9	0.97
		Cd+Ni+Cu	192.06	78.2	0.98
goethite–B. cereus	Cd	Cd alone	128.15	17.3	0.99
		Cd+Ni+Cu	57.50	29.5	0.93
	Ni	Ni alone	134.24	30.0	0.97
		Cd+Ni+Cu	68.67	39.4	0.93
	Cu	Cu alone	179.04	53.4	0.96
		Cd+Ni+Cu	138.70	60.3	0.98

600   [a] Maximal sorption caparicy capacity predicted by Langmuir isotherm. [b] Equilibrium constant related to the

601   binding affinity.

602

603

604

605

606

607

FIGURE CAPTION

609 **Fig. 1.** Scanning electron microscope secondary electron images of goethite (a), *B.*

610 *cereus* cells (b) and goethite–*B. cereus* composites (c and d). EDS spectrum of the

611 labeled region in the goethite–*B. cereus* composite after sorbing Cd, Ni and Cu (e).

612 The table below summarizes the concentration of major elements in the EDS region.

613 **Fig. 2.** Sorption isotherms of Cd, Ni and Cu in single (circle) and ternary (triangle)

614 systems on goethite (top), *B. cereus* cells (middle) and goethite–*B. cereus* composites

615 (bottom). Solid lines are Langmuir model fits.

616 **Fig. 3.** X-ray photoelectron low resolution spectra of goethite–*B. cereus* composite

617 before (a) and after (b) sorbing Cd, Ni and Cu.

618 **Fig. 4.** X-ray photoelectron high-resolution of O1s and C1s spectra for goethite–*B.*

619 *cereus* composite before (a, c) and after (b, d) sorbing Cd, Ni and Cu.

620 **Fig. 5.** Synchrotron-based X-ray fluorescence maps show the distribution of Fe, P, Cu,

621 Ni and Cd within the goethite–*B. cereus* composites. Color scales indicates the

622 elemental content from blue (lowest) to red (highest). The scatterplots in the lower

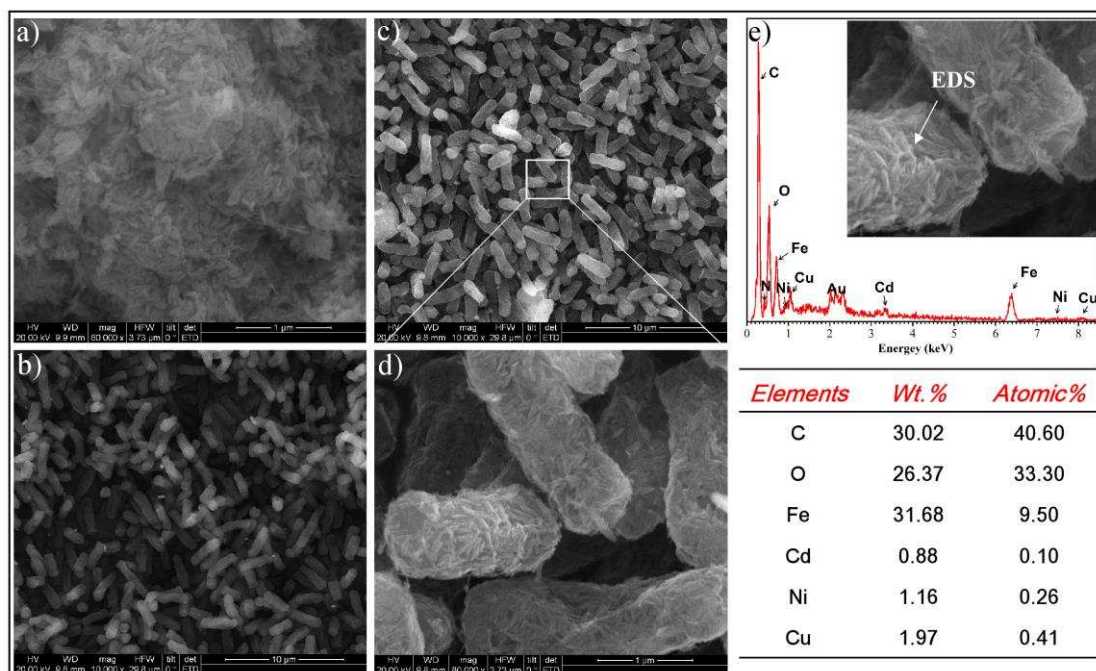623 panels show the correlation between counts of Cu, Cd and Ni *versus* Fe and P.

624

625

626

627

628

629

630   **Fig. 1**
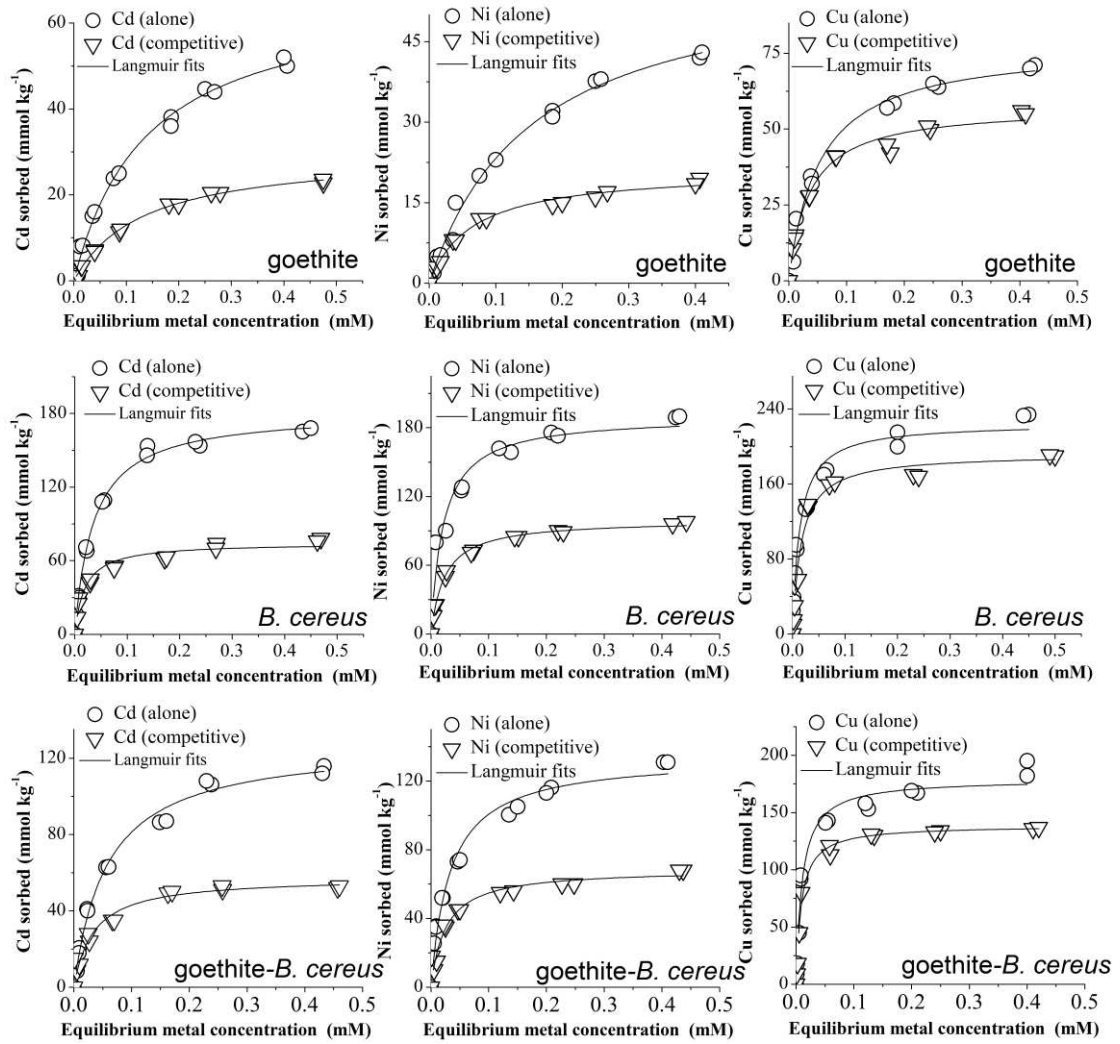

631

632

633

634

635

636

637

638

639

640

641

642

643

644

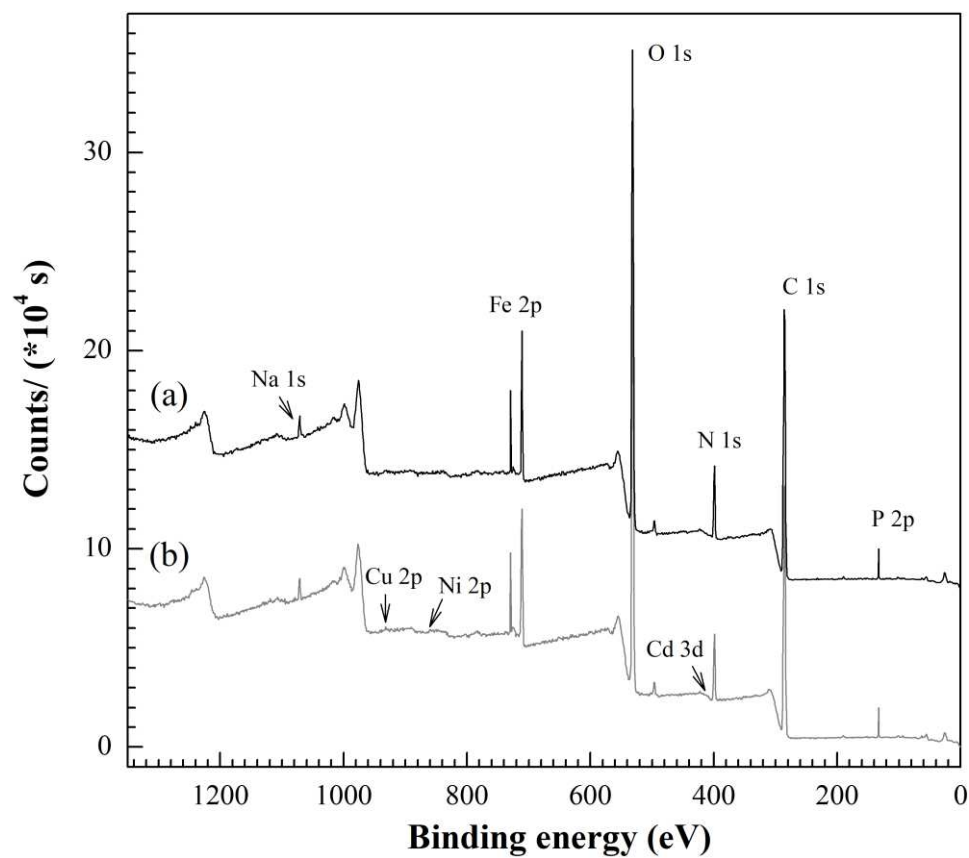645 **Fig. 2**
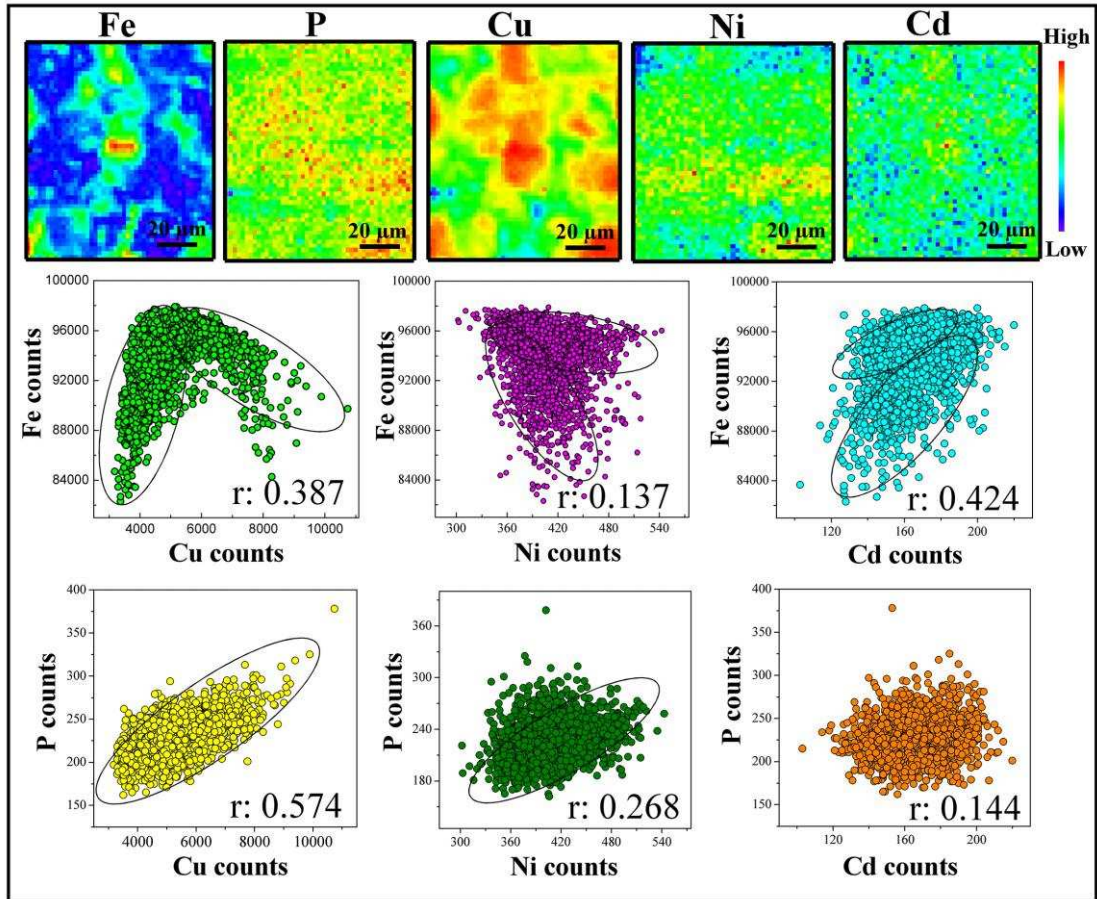
Fig. 3

Fig. 4
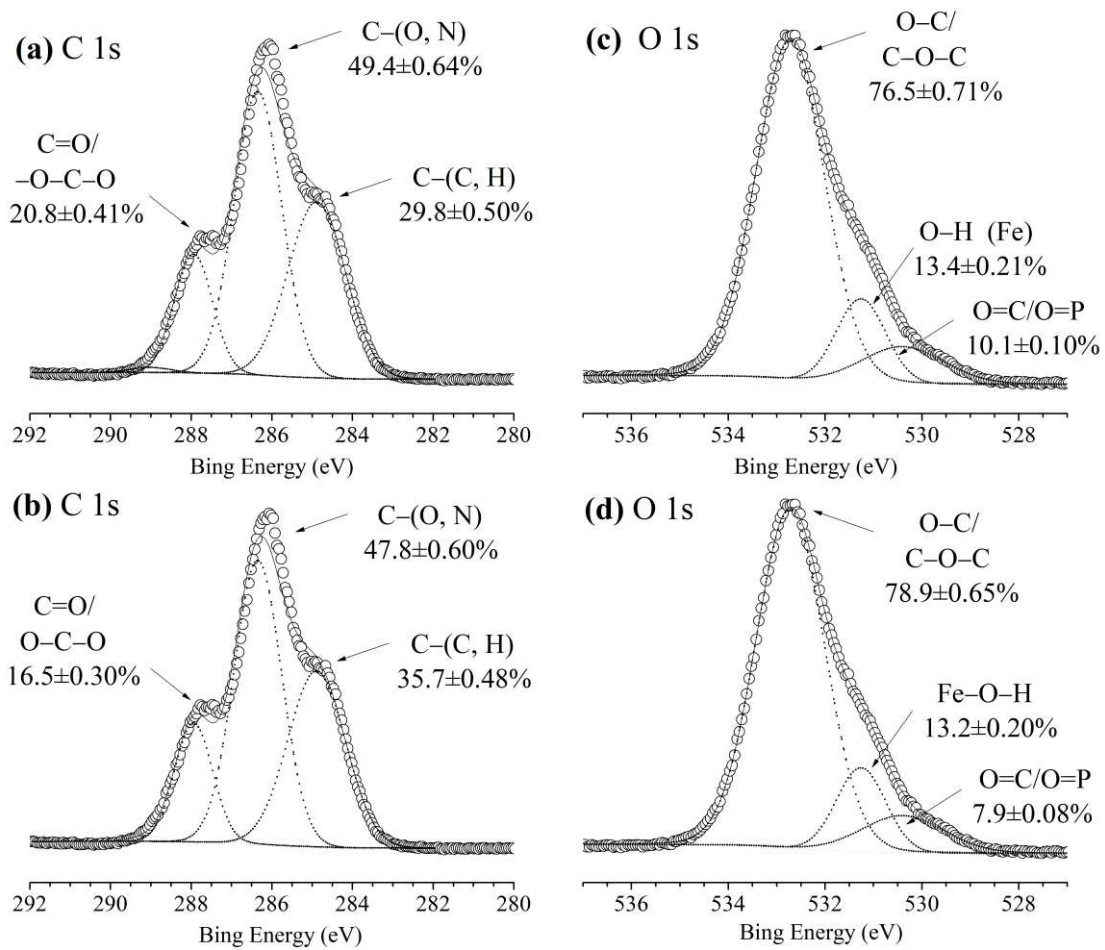
680   **Fig. 5**

681

682

683

684

685

686

687

688

689

690

691